Supporting Information

Gu et al. 10.1073/pnas.1215086110

SI Text

Determination of Kinetic Isotope Effects on RNA 2′-*O*-Transphosphorylation Reactions. Solution and enzyme kinetic isotope effects (KIEs) were measured for the 2′-*O*-transphosphorylation reaction of the dinucleotide uridylyl-(3′,5′)-guanosine (5′-UpG-3′ or UpG) (Fig. 1*B*) to form 2′,3′-cyclic uridine monophosphate (cUMP) and guanosine (G). UpG was synthesized to contain ^{18}O at the 2′O, 5′O, and nonbridging phosphoryl oxygen (NPO) positions, individually. Briefly, the ^{18}O-enriched RNA was synthesized using [$^{18}O_2$]benzoic acid as a nucleophile to deliver the isotopic substitution to activated nucleoside ribose 2′ or 5′ carbons of protected ribonucleosides, followed by hydrolysis of the benzoate ester as described. The [2′-^{18}O]- or [5′-^{18}O]-nucleoside was coupled to commercially available phosphoramidite to yield the RNA dinucleotides [2′-^{18}O]UpG and Up-[5′-^{18}O]G. Up[NPO-^{18}O]G was synthesized by including $H_2{}^{18}O$ in the hydrolysis step during solid phase synthesis (1).

The 2′-*O*-transphosphorylation reaction of UpG catalyzed by specific base was performed as described, and catalysis by specific acid was analyzed similarly (2). Briefly, the reaction of 1–5 nmol of UpG at pH 0 (1 M HCl) was carried out in 250–500 μL at 37 °C. Kinetics were followed by removing aliquots at specific times and neutralizing with an equivalent of NaOH, followed by further dilution with 100–200 μL of 0.1 M ammonium acetate at pH 8.0. For RNase A reactions, the enzyme was removed by centrifugation through Centricon-10 filters (Millipore) and the flow-through was collected.

The reactant (UpG) and products (cUMP and G) were resolved by RP-HPLC on a 300 × 50-mm C18 column run isocratically at 1 mL/min with a mobile phase of 0.1 M ammonium acetate and 4% (vol/vol) acetonitrile. The elution of precursor UpG and products cUMP and G were monitored by UV absorbance at 260 nm (Fig. S2*A*). The fraction of reaction, F = [cUMP or G]/([UpG] + [cUMP or G]), was quantified by integration of the chromatogram. The HPLC fractions containing the unreacted UpG were collected and dried under vacuum. The pellets were resuspended in 1 mL of H_2O, dried down three to four additional times, and finally resuspended in water at a concentration of 20–50 μM for subsequent isotopic analysis by tandem MS.

Determination of the substrate $^{16}O/^{18}O$ ratio in UpG was accomplished by tandem MS using an ABI QStar electrospray ionization quadrupole/TOF tandem mass spectrometer in negative ion mode. The sample was injected at 1–0.5 μL/min using an ion voltage of −2,200 V. The entire deprotonated molecular ion isotopic cluster of the substrate with a monoisotopic m/z of 588 was isolated using low resolution in the initial quadrupole stage and fragmented by inert gas collision at a collision energy of 35 eV. In the second stage, the resulting fragments at 100–600 m/z were resolved by TOF-MS. Fragmentation of the monoisotopic ion yields high-intensity product ions at m/z 476 and m/z 211 that result from loss of the uridine nucleobase and from ribosephosphate, respectively, as shown in Fig. S2*B*. Both species contain the enriched 2′-O, 5′-O NPO positions, and were sufficiently abundant for precise quantitation of $^{16}O/^{18}O$ ratios in the residual substrate population with 10–15 min of continuous data acquisition. The second TOF-MS dimension produces highly enhanced signal to noise as demonstrated in Fig. S2*C* for the 211/213 ion pair. The absence of background noise and the exclusion of contaminants due to the high mass resolution of the TOF result in a precision of 0.5% or better as assessed by analytical dilution of isotopic standards. Fitting the m/z data to a series of Gaussian peaks was used to quantify the abundance of the two isotopologues and to determine the $^{16}O/^{18}O$ ratio (3). Alternatively, with complete baseline separation of the isotopic peaks and the absence of apparent contaminants, the Analyst (Applied Biosystems) integration routine produced equivalent results.

Impact of Binding Commitments on Interpretation of Intrinsic KIEs for RNase A. Because the method described above involves internal competition between two substrates in the same reaction, the observed KIE measures the ratios of the k_{cat}/K_m values for the RNAs containing ^{16}O and ^{18}O (2, 4). Therefore, substrate binding steps may interfere with the KIE measurements for RNase A if dissociation is slow relative to chemistry, resulting in a "commitment" of the bound substrate to undergo the chemical transformation (5). Here, we consider in more detail the meaning of k_{cat}/K_m for the UpG substrate under conditions where KIEs were measured, and the potential impact of binding commitments on the observed experimental KIE values was assessed. For the simplest mechanism in which a single form of the enzyme combines with the substrate [i.e., the middle pathway for reaction of the correctly protonated form of the enzyme (EH) and substrate (S) in Scheme **S1**, below], the

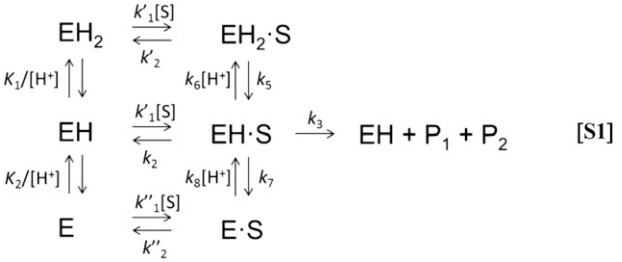

[S1]

reaction at limiting substrate concentration can be considered to follow a simple rate equation (6),

$$\frac{k_{cat}}{K_m} = \frac{k_1 k_3}{k_2 + k_3},$$

where k_1 and k_2 represent the rate constants for substrate association and dissociation, respectively, and k_3 is the rate constant for the conversion of bound substrate to free enzyme and product in this case. Conditions under which substrate dissociation is fast relative to the chemical step of the reaction ($k_2 > k_3$) are most favorable for measuring enzyme KIEs. Under these circumstances,

$$\frac{k_{cat}}{K_m} = \frac{k_1 k_3}{k_2 + k_3} = \frac{k_1 k_3}{k_2} = \frac{k_3}{K_d},$$

where K_d is the equilibrium dissociation constant for substrate binding. Therefore, because isotope effects express the ratio of k_{cat}/K_m values, they report on the difference in bonding between the substrate free in solution and in the transition state, and they can include effects on binding as well as the chemical step (7).

Alternatively, a sticky substrate, or one that can be described as having a high binding commitment, is defined as one that reacts through the first irreversible step of the reaction (k_3) with a rate constant that is faster than the rate constant for dissociation (k_2) (4, 8). The commitment factor or stickiness ratio (C) is defined as k_3/k_2 for the simple mechanism above. Under these circumstances, the observed KIE is attenuated proportionally according to Cleland and Cook (4) and Cleland (8): $^{18}k_{obs} = (^{18}k + C)/(1 + C)$.

Given this relationship, a commitment factor of *ca.* 2 would reduce an intrinsic leaving group KIE of *ca.* 1.035 to a value that is observed for RNase A (*ca.* 1.015). A proportional attenuation of the value of the observed RNase A nucleophile KIE ($^{18}k_{NUC}$; 0.994) due to a binding commitment of this magnitude would result in an intrinsic $^{18}k_{NUC}$ with an estimated magnitude of 0.988. As described in the text, the $^{18}k_{NUC}$ for this reaction is interpreted as resulting from the combined effects of O-P bond formation and deprotonation. It seems unlikely that a more inverse $^{18}k_{NUC}$ value could result from increased O-P bonding, considering that the acid-catalyzed reaction, which is fully stepwise, shows a similar inverse $^{18}k_{NUC}$ (Table 1). Also, computational models involving a transient phosphorane intermediate with advanced 2′O-P bonding are consistent with the observed KIEs (1, 9). Because the equilibrium isotope effect (EIE) for deprotonation is normal (1.015–1.024) in the direction of deprotonation, incomplete deprotonation of the 2′O would result in only partial expression of this effect in the transition state. The net effect could be a more inverse $^{18}k_{NUC}$ due to a smaller normal contribution to the observed intrinsic KIE from loss of the O-H bonding vibrational mode. However, any mechanistic scenario must necessarily account for the large (1.035) KIE on the 5′O leaving group. Taken together, these results would imply that the departure of the 5′O occurs as an oxyanion with little participation of active site functional groups offsetting the buildup of unfavorable negative charge by protonation. Thus, the estimated 2′O and 5′O KIEs, assuming attenuation of both by substrate binding commitments, do not easily correspond with expectations based on the observed solution KIEs and the proposed mechanism of RNase A from previous structural and mechanistic work.

Analysis of the Binding Commitment for UpG Cleavage by RNase A. Several experimental observations can be considered to gain information on the degree to which binding commitments affect the observed KIEs for RNase A. These data can include (*i*) comparison of the magnitude of observed RNase A effects relative to intrinsic KIEs on solution reactions and to values previously measured for a slow substrate, (*ii*) comparison of the reaction kinetics of UpG with those of other model substrates, (*iii*) analysis of the effects of solvent viscosity, and (*iv*) evaluation of the difference between the microscopic pK_a values of active site residues measured directly and observed macroscopic pK_a values from kinetic studies. The experimental data relating to these factors are discussed, in turn, below.

Importantly, the observation that the KIEs for RNase A are similar in magnitude to the values observed for solution reaction, where binding commitments are not present, argues that the chemical step is at least partially rate-limiting. This interpretation could also be consistent with the scenario described above, where the commitment factor is small and only partial expression of the intrinsic KIE is observed. Nonetheless, the leaving group KIE reported here for UpG (1.014) is similar to the value measured for uridine 3′-*m*-nitrobenzyl phosphate (1.017) reported by Cleland and colleagues (10). This slow substrate reacts with a k_{cat}/K_m that is 10^4-fold lower than uridylyl-3′-adenosine [5′-UpA-3′ (UpA)] and 10^3 lower than UpG. Thus, the correspondence of the observed KIEs for the RNase A reaction reported here with the previously reported KIEs for solution reactions and previous effects for RNase A using a model substrate is consistent with the conclusion that the observed KIEs closely approximate the intrinsic effects.

Perspective on the rate-limiting steps for the UpG reaction can also be gained by comparing the kinetic parameters of UpG with those determined for other RNase A substrates. The k_{cat} for the reaction of UpG is ~30 s^{-1} (Fig. S3), which is significantly slower than UpA (1,400 s^{-1}) under similar reaction conditions (11). The k_{cat} for uridine 3′-*p*-nitrophenol phosphate is approximately twofold slower (19 s^{-1}) (12). The rate constant for release of a cyclic nucleotide monophosphate is 1,500 s^{-1} and has been proposed to be rate-limiting for k_{cat} for fast-reacting polynucleotide substrates and for UpA (11, 13). The observed k_{cat} for UpG is significantly slower and presumably represents a slow step upstream of substrate dissociation. The k_{cat}/K_m for UpG is 2.7×10^4 $M^{-1}\cdot s^{-1}$, which is significantly less than the k_{cat}/K_m for a UpA substrate (2.3×10^6 $M^{-1}\cdot s^{-1}$) and similar to the value of 5.7×10^4 $M^{-1}\cdot s^{-1}$ observed for uridine-3′-*p*-nitrophenol phosphate measured under similar conditions (11, 12, 14). Therefore, the low magnitude of k_{cat} for the UpG reaction relative to the k_{cat} values for UpA and oligonucleotide substrates makes it unlikely that product release is rate-limiting, and the k_{cat}/K_m for UpG is consistent with other slow-reacting substrates for which the chemical step is considered to be rate-limiting.

The stickiness of a substrate will also affect the observed pH profile of the reaction (4, 15), and the quantitative nature of the dependence is determined by the specific kinetic scheme (16, 17). The following kinetic scheme from Park and Raines (11) is assumed for the reaction of UpG by RNase A under k_{cat}/K_m (limiting substrate concentration) conditions. Similar to other substrates, the observed pH dependence of k_{cat}/K_m for the reaction of the UpG substrate (Fig. S4) is consistent with a mechanism in which there are two titratable groups important for the reaction.

The acid dissociation constants for protonation of the two functional groups assumed to be His12 and His119 are K_1 and K_2, and the second-order rate constants for association of the substrate are k_1, k'_1, and k''_1. The first-order rate constants for substrate dissociation are k_2, k'_2, and k''_2, and the chemical step is k_3. The rate equation for k_{cat}/K_m is

$$\frac{k_{cat}}{K_m} = \frac{\left(k'_1\frac{[H^+]}{K_1} + k_1 + k''_1\frac{K_2}{[H^+]}\right)k_3}{\left(\frac{[H^+]}{K_1} + 1 + \frac{K_2}{[H^+]}\right)\left(\frac{k'_2k_6[H^+]}{k'_2 + k_5} + k_2 + k_3 + \frac{k''_2k_7}{k'_2 + k_8[H^+]}\right)}.$$

If it is assumed that proton association and dissociation are rapid relative to substrate binding rate constants, the rate equation simplifies to

$$\frac{k_{cat}}{K_m} = \frac{\left(k'_1\frac{[H^+]}{K_1} + k_1 + k''_1\frac{K_2}{[H^+]}\right)k_3}{\left(\frac{[H^+]}{K_1} + 1 + \frac{K_2}{[H^+]}\right)\left(k'_2\frac{[H^+]}{K'_1} + k_2 + k_3 + k''_2\frac{K'_2}{[H^+]}\right)},$$

where K'_1 and K'_2 are the acid dissociation constants in the presence of the bound substrate. The issue of whether the protons bound to the RNase A active site are themselves sticky in the presence of the bound substrate is not known. However, given the slow reactivity of the UpG substrate and the fact that the dynamic motions of the enzyme occur with much faster rate constants, this assumption appears reasonable. If the substrate is not sticky and k_2 is large, the rate equation reverts to its simple form, which is used to fit the pH profile data in Fig. S4. The observed kinetic pK_a values are assumed to approximate the intrinsic enzyme acid dissociation constants K_1 and K_2 in Scheme **S1**.

As described previously (4, 11, 15), for a sticky substrate, the presence of binding commitments can result in alteration of the pH profile of the reaction such that the observed macroscopic pK_as do not correspond to the intrinsic microscopic pK_as of the titratable groups involved in the reaction. The observed macroscopic pK_a for the reaction of UpG is 5.2, whereas the predicted pK_a under similar reaction conditions is 5.6, as described previously by Park and Raines (11). If the observed macroscopic pK_a represents His12, the difference between these values is an estimation of the binding commitment according to the following: $pK_{app} = pK_1 - \log(1 + C)$.

Thus, the difference of 0.4 between the observed and predicted pK_a values could potentially reflect a small binding commitment of ~1.5. A substrate binding commitment of this magnitude would be sufficient to reduce an intrinsic KIE of 1.035 to the value of 1.014 observed for RNase A as discussed above. On the other hand, the observed pK_a for the acidic functional group, assumed to be His119, is 6.3, which is less than the predicted value of 6.6. The presence of a significant binding commitment would result in an apparent increase in the pK_a in this instance, and this expectation does not hold. Thus, these data indicate that under conditions in which KIE measurements were performed at pH 7, which is above the pK_a of the general acid, the substrate binding commitments are minimal.

However, as pointed out previously (11), there are two scenarios in which the substrate can be sticky and there will still be minimal effect on the observed pK_a relative to its intrinsic value. The first occurs if release of the proton from EH·S (k_7) is slow relative to substrate dissociation (k_2); however, as indicated above, this is unlikely to be the case for the UpG substrate. The second occurs when the rate constant for association with EH is much faster than with the form of the enzyme in which neither active site functional groups are protonated (E) ($k_1 > k''_1$). Although the magnitudes of the rate constants for association of substrates with the different protonated forms of the enzyme are not known, the binding of the anionic substrate to the mono- or deprotonated active site is likely to occur with a greater rate constant than to the fully deprotonated form. Indeed, the higher affinity of an oligodeoxynucleotide substrate mimic at low pH has been demonstrated previously (18). Thus, although these data do not provide direct evidence for the relative magnitudes of k_3 and k_2, the observed pH dependence of the reaction is consistent with mechanisms in which there are minimal binding commitments.

The effect of viscosity on k_{cat}/K_m values can also provide information on substrate stickiness. In the mechanism shown above, the chemical step k_3 is independent of solvent viscosity (because it is intramolecular within the active site), and steps associated with substrate binding and product dissociation are assumed to be inversely proportional to the solvent viscosity. Accordingly, if viscosity does not affect k_{cat}/K_m, this result is consistent with low binding commitments because it is assumed that viscosity equally affects k_1 and k_2. If product release limits k_{cat}/K_m, the observed rate will decrease even if the substrate is not sticky. As shown in Fig. S5, the k_{cat}/K_m of the UpG substrate is essentially insensitive to concentrations of glycerol, which increase the solution viscosity sufficiently to perturb macromolecular association and dissociation processes. Therefore, the insensitivity of the observed k_{cat}/K_m to viscosity under the conditions in which KIEs were measured is consistent with a mechanism in which there are low binding commitments and the product release step is not rate-limiting. As indicated above, the k_{cat} for UpG is significantly slower than the protein dynamics that are proposed to be rate-limiting for fast substrates. As demonstrated by Thompson (12), the k_{cat}/K_m for the faster UpA substrate decreases with increasing solvent viscosity in a manner consistent with rate-limiting substrate association, whereas the reaction of uridine-3′-*p*-nitrophenol phosphate was not sensitive. Therefore, the observed insensitivity of the UpG reaction to increasing glycerol is consistent with a mechanism in which a step other than association or product release is rate-limiting.

Computational Evaluation of Alternative Transition State Models. To define the structure of the RNase A transition state better and evaluate the potential for active site interactions to influence charge distribution and the resulting KIEs, we analyzed a total of five models: two nonenzymatic models and three enzymatic models. The transition states of these five models are depicted in Fig. S6, whereas their calculated KIE values are listed in Table S1. The results with these five model systems were used to guide the quantum mechanical calculations presented in the main text, which involve a more complex structure, including the adjacent ribose structure, as shown in Fig. S4.

The first nonenzymatic model (denoted as 1stNonEnzyme in Fig. S6) is an ethylene glycol phosphate methyl ester reacting under alkaline conditions. In this model, we assume that the deprotonation occurs in a preequilibrium that is not rate-limiting. As seen in Table S1, the calculated KIEs for this model are consistent with experimental results for the base-catalyzed 2′-*O*-transphosphorylation of the RNA dinucleotide 5′-UpG-3′ (2). More details and discussions, as well as further insights provided by this model and other relevant models, can be found in the paper by Wong et al. (1).

In the second nonenzymatic model (denoted as 2ndNonEnyzme in Fig. S6), we examined the effect of adding a proton at O2′ in the reactant state. This model was constructed to evaluate the potential for a proton transfer first from O2′ to O1P and then from the O1P position to the 5′O leaving group in the rate-limiting transition state of the solution reaction catalyzed by specific acid. In comparison to the first nonenzymatic model, the KIE value of the leaving group ($^{18}k_{LG}$) drops from 1.059 to 1.046 due to the concomitant proton transfer. This suggested that the decreased magnitude of $^{18}k_{LG}$ relative to the specific base reaction could also be due to concomitant proton transfer (i.e., general acid catalysis). However, the lack of a large thio effect on the RNase A reaction and the relatively smaller normal value of $^{18}k_{LG}$ we observe both argue against complete proton transfer from an NPO position to the 5′O leaving group in the RNase A reaction.

Consequently, based on our second nonenzymatic model mentioned above, which has a proton at O2′ in the reactant state, we built our first enzymatic model (denoted as 1stEynzme in Fig. S6) by testing the effect of adding a single protonated imidazole. This protonated imidazole is hydrogen-bonded with O5′ in the reactant state and transfers a proton to O5′ in the transition state. This model was constructed to probe the possibility of a proton transfer from O2′ to an NPO, followed by proton transfer from the protonated imidazole (instead of from the NPO) to the 5′O leaving group. In other words, the protonated imidazole is the general acid and the proton at O1P does not move in the rate-limiting transition state of our first enzymatic model (Fig. S6). As seen in Table S1, in contrast to our second nonenzymatic model, the value of $^{18}k_{LG}$ significantly drops from 1.046 to 1.010. This indicates substantial offset of the magnitude of this KIE by concomitant proton transfer in the transition state of which the protonated imidazole acts as the general acid and O1P stays protonated. However, the calculated KIE value of the NPO effect ($^{18}k_{NPO}$) is small and inverse this time (Table S1), which is inconsistent with the experimentally observed small normal values. Again, the lack of a large thio effect on the RNase A reaction and the small normal value of $^{18}k_{NPO}$ we observe both argue against protonation at an NPO position in the rate-limiting transition state in the RNase A reaction.

Therefore, we built the second and the third enzymatic models (denoted as 2ndEynzme and 3rdEnzyme, respectively, in Fig. S6) to test the effect of removing the proton at the O1P position in the transition state. In addition, in our third enzymatic model, we positioned a second protonated imidazole ring that is hydrogen-bonded with O1P in the transition state (Fig. S6). Initially, we had a hard time locating a late transition state for the 2ndEynzme model because the potential energy surface is quite flat. In contrast, the transition state was readily identified for our third enzymatic model. Moreover, this model most closely approximates the observed RNase A KIEs (Table S1), which show a normal value for $^{18}k_{LG}$, near-inverse unity for $^{18}k_{NUC}$, and near-normal unity for $^{18}k_{NPO}$. Therefore, the enzymatic model presented in Fig. 4 was built with two protonated imidazoles based on the results from the 3rdEynzme model. One imidazole is hydrogen-bonded with O1P, and another functions as the gen-

eral acid for the 5′O leaving group in the transition state. The model in Fig. 4 also includes a more realistic ribose-like sugar ring and ethoxide leaving group. This model supports a scenario that His12 (or other candidates) accepts a proton from O2′, Lys41 (or His12 or other candidates) H-bonded with NPO and that His119 donates the proton to the leaving O5′.

Moreover, our approach for modeling the transitions states for solution and RNase A-catalyzed RNA 2′-*O*-transphosphorylation reactions differs from previous methods used to model the transition states by Schramm and colleagues (19). The transition states modeled in the present study are fully optimized without any constraint, including without the constraint of matching the experimental KIE values. By definition, a transition state should be at a stationary point of the reactive potential energy surface, that is, at a point where the force or gradient of the potential energy surface is zero. Additionally, it should have only a single imaginary frequency. Both of these criteria are met by the transition states reported in this work. From our previous work, we showed that the hybrid B3LYP exchange correlation density functional is accurate enough for successfully characterizing the reaction paths and transition states, as well as the effects of thio substitutions on the nonbridging oxygens (1).

1. Wong KY, et al. (2012) Characterization of the reaction path and transition states for RNA transphosphorylation models from theory and experiment. *Angew Chem Int Ed Engl* 51(3):647–651.
2. Harris ME, et al. (2010) Kinetic isotope effects for RNA cleavage by 2′-O-transphosphorylation: Nucleophilic activation by specific base. *J Am Chem Soc* 132(33):11613–11621.
3. Cassano AG, et al. (2007) Inaccuracies in selected ion monitoring determination of isotope ratios obviated by profile acquisition: Nucleotide 18O/16O measurements. *Anal Biochem* 367(1):28–39.
4. Cleland WW, Cook PF (2007) *Enzyme Kinetics and Mechanism* (Garland, New York).
5. Cleland WW (2005) The use of isotope effects to determine enzyme mechanisms. *Arch Biochem Biophys* 433(1):2–12.
6. Cleland WW (1975) Partition analysis and the concept of net rate constants as tools in enzyme kinetics. *Biochemistry* 14(14):3220–3224.
7. Schramm VL (2007) Binding isotope effects: Boon and bane. *Curr Opin Chem Biol* 11(5):529–536.
8. Cleland WW (1982) Use of isotope effects to elucidate enzyme mechanisms. *CRC Crit Rev Biochem* 13(4):385–428.
9. Radak BK, Harris ME, York DM (2013) Molecular simulations of RNA 2′-O-transesterification reaction models in solution. *J Phys Chem B* 117(1):94–103.
10. Sowa GA, Hengge AC, Cleland WW (1997) 18O isotope effects support a concerted mechanism for ribonuclease A. *J Am Chem Soc* 119(9):2319–2320.
11. Park C, Raines RT (2003) Catalysis by ribonuclease A is limited by the rate of substrate association. *Biochemistry* 42(12):3509–3518.
12. Thompson JE, et al. (1995) Limits to Catalysis by Ribonuclease A. *Bioorg Chem* 23(4): 471–481.
13. Watt ED, Shimada H, Kovrigin EL, Loria JP (2007) The mechanism of rate-limiting motions in enzyme function. *Proc Natl Acad Sci USA* 104(29):11981–11986.
14. Thompson JE, Raines RT (1994) Value of general Acid-base catalysis to ribonuclease a. *J Am Chem Soc* 116(12):5467–5468.
15. Cleland WW (1977) Determining the chemical mechanisms of enzyme-catalyzed reactions by kinetic studies. *Adv Enzymol Relat Areas Mol Biol* 45:273–387.
16. Cook PF, Cleland WW (1981) pH variation of isotope effects in enzyme-catalyzed reactions. 1. Isotope- and pH-dependent steps the same. *Biochemistry* 20(7):1797–1805.
17. Cook PF, Cleland WW (1981) pH variation of isotope effects in enzyme-catalyzed reactions. 2. Isotope-dependent step not pH dependent. Kinetic mechanism of alcohol dehydrogenase. *Biochemistry* 20(7):1805–1816.
18. Park C, Schultz LW, Raines RT (2001) Contribution of the active site histidine residues of ribonuclease A to nucleic acid binding. *Biochemistry* 40(16):4949–4956.
19. Schramm VL (2011) Enzymatic transition states, transition-state analogs, dynamics, thermodynamics, and lifetimes. *Annu Rev Biochem* 80:703–732.

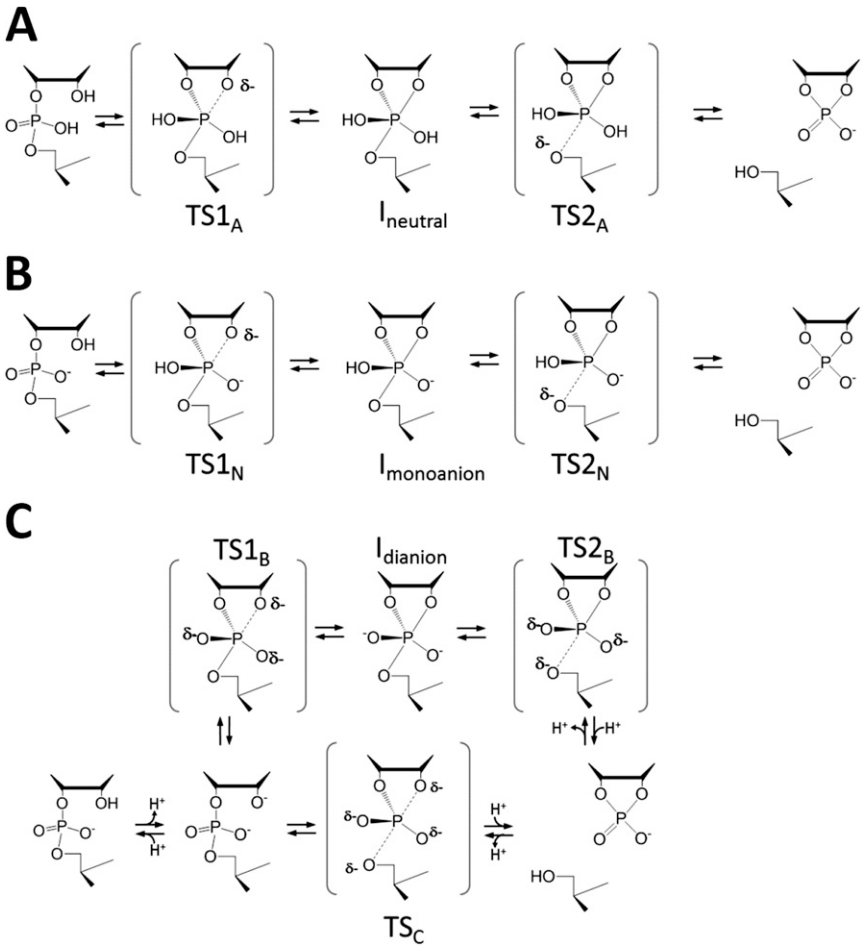

Fig. S1. Potential reaction schemes for RNA 2′-*O*-transphosphorylation. (*A*) Stepwise mechanism for acid catalysis involves the formation of a neutral phosphorane intermediate ($I_{neutral}$). (*B*) Stepwise mechanism for acid catalysis with formation of a monoanionic phosphorane intermediate ($I_{monoanion}$). (*C*) Concerted and stepwise mechanism with formation of an anionic phosphorane intermediate ($I_{dianion}$) for base catalysis. TS, transition state.

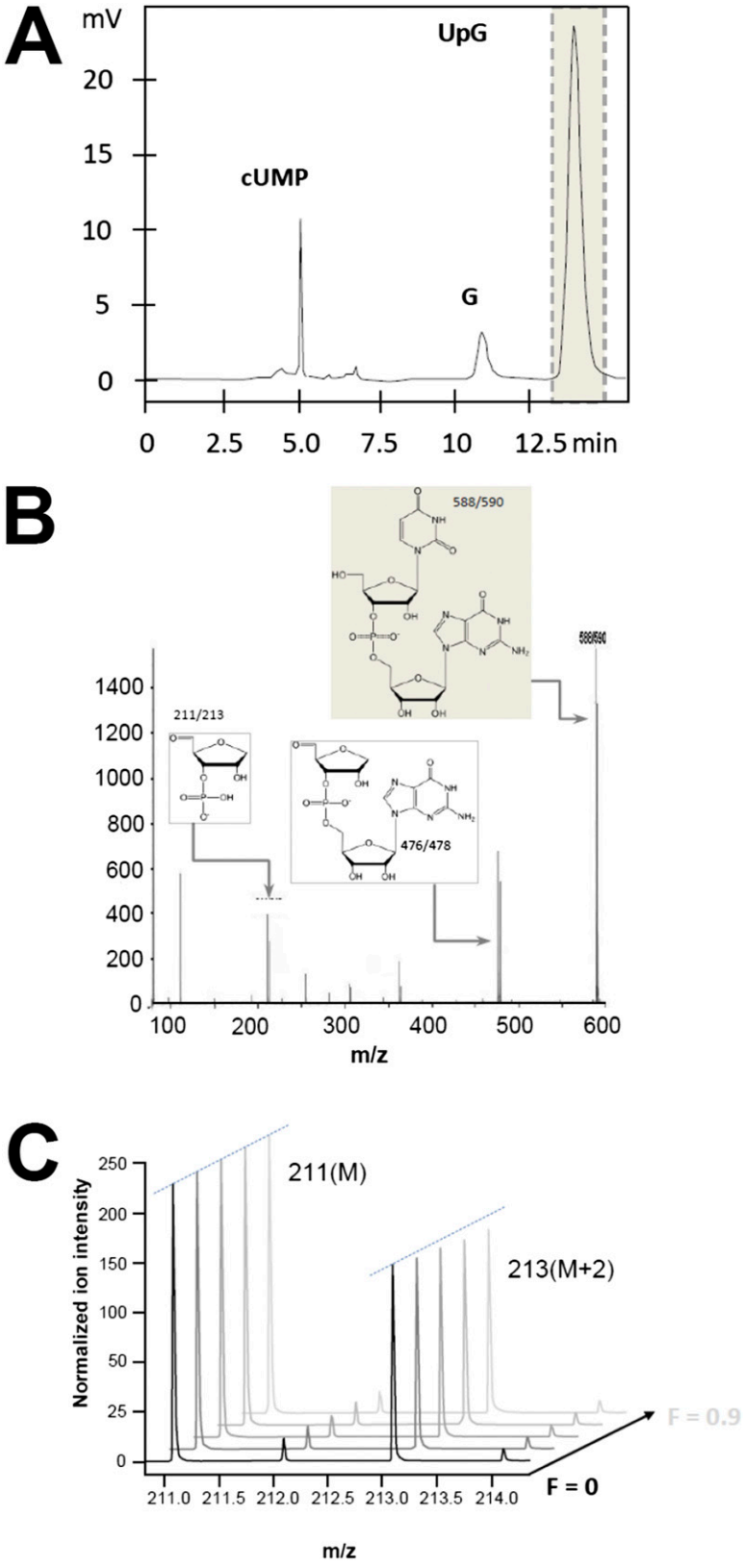

Fig. S2. Determination of KIEs on RNA 2′-*O*-transphosphorylation reactions by internal competition. (*A*) RP-HPLC separation of substrate UpG and products cUMP and G. (*B*) TOF product ion spectrum of UpG showing the *m/z* 211/213 and 476/478 ions used to compute $^{18}O/^{16}O$ isotope ratios. The structures of the molecular ion *m/z* 588/590 and product ions used to compute the KIEs are shown. (*C*) Close-up of mass spectrum of the *m/z* 211/213 product ions showing the high level of signal to noise, consistent peak shape, and mass resolution obtainable. A cartoon of overlain spectra is shown, indicating results from samples for the same reaction that are analyzed at early (black, dark gray) and progressively higher fractions of reaction (progressively lighter gray). The change in the relative areas of the 211 (M) and 213 (M + 2) peaks is used to compute the isotope effect. The relative heights of the two peaks are indicated by dashed lines.

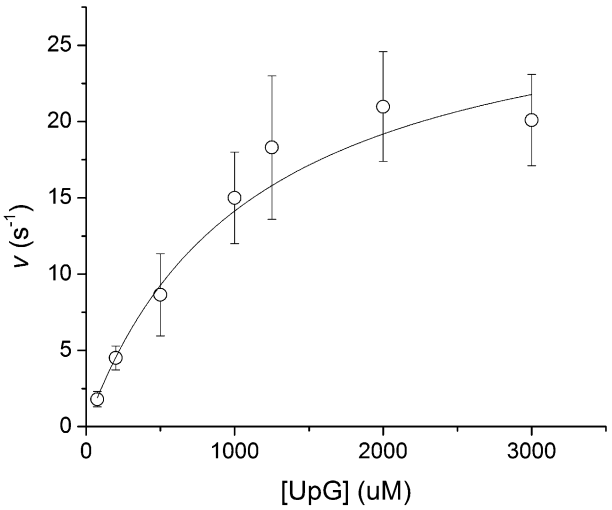

Fig. S3. Multiple turnover kinetics of UpG cleavage by RNase A. The steady-state reaction rates (v_{obs}/E_{total}) were determined at substrate concentrations ranging from 75 to 3,000 μM UpG in 0.1 M NaCl, 10 mM bis-Tris (pH 7.0), and 40 nM enzyme. The conversion of substrate UpG to product cUMP and G was quantified by analysis of reaction time points by RP-HPLC as shown in Fig. S2*A,* followed by integration of the chromatograms to determine the fraction of reacted substrate. Initial rates were determined from the slope of linear fits of the fraction of the reacted substrate vs. time at less than 10% conversion of the total substrate concentration. These data were fit to the Michaelis–Menton equation [$v = k_{cat}/(1 + K_m/[UpG])$] to estimate k_{cat} ($30 \pm 3\ s^{-1}$), K_m (1,100 ± 200 μM), and k_{cat}/K_m [2.7 (±0.8) × 10^4 $M^{-1}{\cdot}s^{-1}$).

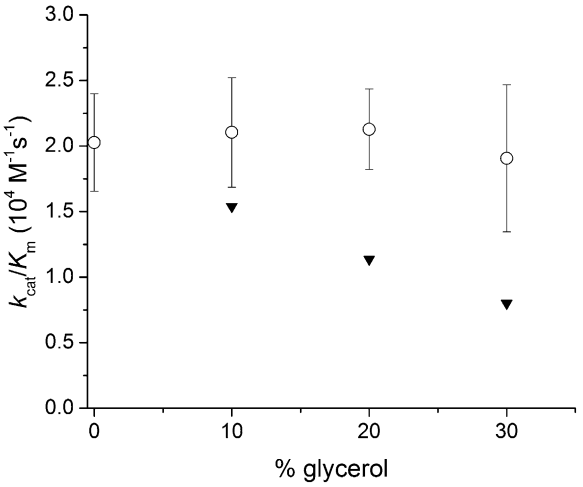

Fig. S4. Dependence of k_{cat}/K_m on glycerol concentration. The steady-state reaction rates (v_{obs}/E_{total}) were determined as described in the legend for Fig. S3, with the exception that conversion of UpG to product was quantified using UV absorbance spectroscopy. Solutions of enzyme and substrate at 2× concentration were mixed by stopped flow using an Applied Photophysics pi*-180 spectrometer, and the change in absorbance at 260 nm was monitored. Due to the decreased absorbance in the UpG substrate relative to the free nucleoside and nucleotide products, the absorbance increases on product formation. The Δε was determined by taking spectra (220–350 nm) of samples before and after the reaction, with the complete conversion to product confirmed by RP-HPLC. The observed k_{cat}/K_m values in the absence of glycerol and in the presence of increasing glycerol concentrations are shown.

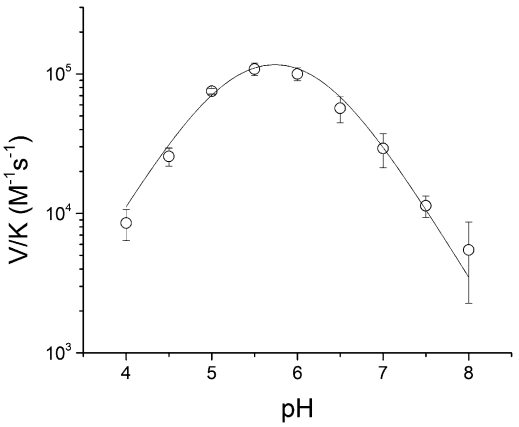

Fig. S5. Dependence of k_{cat}/K_m on pH. The observed k_{cat}/K_m values for steady-state reactions of UpG were determined at pH values from 4 to 8 as described in the legend for Fig. S3, with the exception that buffers at different pH values were used. Conversion of UpG to product was quantified by UV spectroscopy as described in Fig. S4. The following buffers were used: pH 4–4.5, acetate; pH 5–6.5, MES; and pH 7–8, Tris. To estimate the macroscopic pK_a values, the data were fit to $k_{cat}/K_m = (k_{cat}/K_m)_{max}/(1 + 10^{(pH-pK1)} + 10^{(pK2-pH)})$, where the values of pK1 and pK2 are interpreted according to the mechanism discussed in *SI Text* and correspond to the acid dissociation constants K_1 and K_2 in Scheme **S1**.

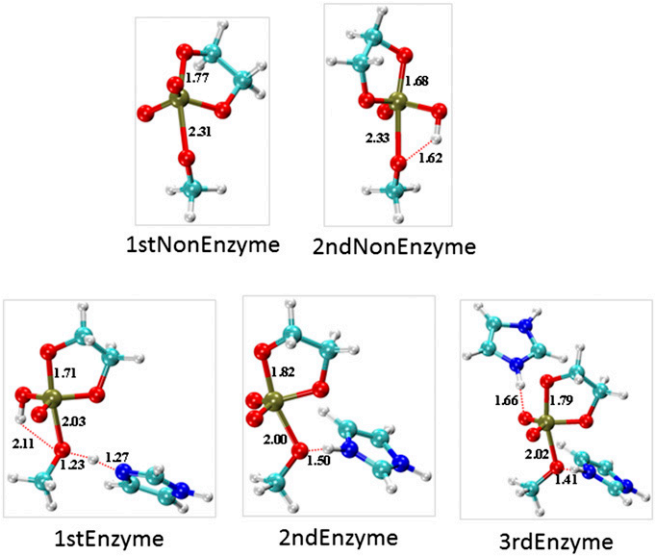

Fig. S6. Alternative solution and enzymatic models. (*Upper*) Two nonenzyme models, 1stNonEnzyme and 2ndNonEnzyme, are shown. (*Lower*) Three enzyme models, 1stEnzyme, 2ndEnzyme, and 3rdEnzyme, are shown. The rationales for construction of these models and the resulting computed KIE values are described in *SI Text*. Key bond lengths are indicated in angstroms.

Table S1. Comparison of calculated KIEs for enzymatic and nonenzymatic models of RNA 2′-O-transphosphorylation

Model system	$^{18}k_{LG}$	$^{18}k_{NUC}$	$^{18}k_{NPO}$
QM nonenzymatic model			
1stNonEnzyme	1.059	0.968	1.004
2ndNonEnzyme	1.046	0.990	1.000
QM enzymatic model			
1stEnzyme	1.010	0.988	0.995
2ndEnzyme	1.038	0.997	1.006
3rdEnzyme	1.037	0.995	1.004
RNase A	1.014	1.014	1.001

QM, quantum mechanics.